East West University

Assignment

Course Code: EEE 308

Course Name: Electronic Properties of Materials

Submitted to:

Shovon Talukder

Dept. of Electrical and Electronic Engineering

East West University

Submitted by:

Name	*ID*
Md. Srabon Islam Ramim	*2020-2-80-046*

Date of Submission: 21-08-2023

Objective: The objective of this assignment is to design and model an electrical/electronic device while emphasizing the selection of materials and understanding their electronic properties. For this assignment Numerical analysis of earth-abundant Cu2ZnSn(SxSe1-x)4 solar cells based on Spectroscopic Ellipsometry results has been conducted by using SCAPS-1D software. The use of renewable energy sources, especially solar photovoltaics (PV), has become essential in the current climate change crisis. The potential energy from the sun is the highest of all renewable sources, and the earth's surface receives enough energy from the sun in just one hour to cover all of humanity's energy needs for a year. Four generations of solar cells can be distinguished, starting with the first generation (1G) based on crystalline silicon (c-Si) and GaAs. Second generation (2G) also known as thin film such as CIGS, amorphous silicon (a-Si) and CdTe. Third generation (3G) as emerging solar cell technologies such as CZTSSe, DSSC and Quantum dot, and new fourth generation (4G) solar cells also known as "inorganics in organics" such as hybrid perovskite. CZTS was first studied as a solar cell material in 1988 at Shinshu University in Japan. Researchers used sputtering to fabricate CZTS thin films and reported p-type conductivity, a direct band gap of 1.45 eV, and an absorption coefficient greater than 104 cm in the visible region. The following year they claimed a solar cell with a Voc of 0.165 V, but with a relatively low Jsc. The first solar cells with efficiencies above 0.6% were reported in 1996 based on CZTS and CZTSe absorbers and cadmium sulfide/zinc oxide window layers. Over the next 10 years, researchers improved processing conditions and window layers, resulting in an efficiency of 7%. At the same time, research on cell solution treatment of CZTSSe began.

In this assignment, the buffer state material has been changed. In the proposed paper buffer layer material was n: CdS. To address Co3 another simulation has been conducted using n: CdZnS as a buffer layer and a comparison between n:CdS and n:CdZnS has been shown.

Diagram of the device:

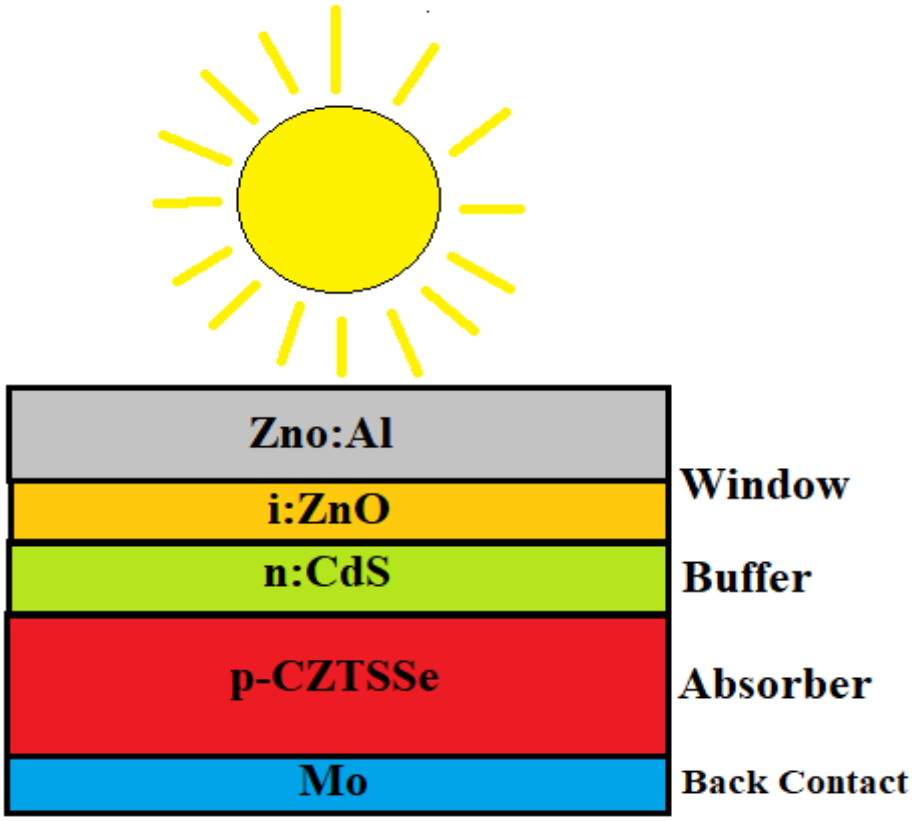

Fig. 1. Schematic diagram of the device

Simulation parameter table:

Table 1: Physical parameters of each layer used in the simulation of CZTSSe.

Material properties	ZnO:Al	i-ZnO	n-CdS	CZTSSe	n_CdZnS
Thickness of the layer(nm)	200	50	50	1900(Varied)	20
Band gap (eV)	3.3	3.3	2.4	1.085(Varied)	2.58
Electron affinity(eV)	4.4	4.4	4.2	4.5(Varied)	4.5
Di electric permeability(eV)	9	9	10	13.6	9.3
Effective density of conduction band(cm^{-3})	2.2×10^{18}	2.2×10^{18}	2.2×10^{18}	2.2×10^{18}	2.4×10^{17}
Effective density of valance band(cm^{-3})	1.8×10^{19}	1.8×10^{19}	1.8×10^{19}	1.8×10^{19}	1.8×10^{18}
Thermal velocity of e^- (cm/s)	10^7	10^7	10^7	10^7	10^7
Thermal velocity of hole (cm/s)	10^7	10^7	10^7	10^7	10^7
Thermal mobility of e^- (cm/Vs)	10^2	10^2	10^2	10^2	85
Thermal mobility of hole (cm/Vs)	2.5×10^1	2.5×10^1	2.5×10^1	2.5×10^1	3.0×10^1
Donor densities	10^{20}	10^{19}	10^{20}	0	1.7×10^{20}
Acceptor densities	0	10^{19}	0	10^{18}	0

Physics: Solar cells transform light energy into electrical energy either indirectly through heat conversion or directly through the photovoltaic effect. In the photovoltaic effect, which happens when light falls on a multilayer semiconductor material, Incoming light with wave-like qualities is focused by mirrors and lenses as it passes through the silicon wafer. Once within the cell, it collides with electrons, knocking them loose and liberating them with particle-like qualities is the basis for the most common types of solar cells. The voltage generated in the cell can drive a current through an external electrical circuit, which can then be used to power electrical equipment. CZTS, like other semiconductor materials such as silicon and CIGSe, may crystallize in a zincblende-derived structure. This kesterite CZTS cell is conceptually generated by replacing half of the In/Ga sites in CIGSe with Zn and the other half with Sn. CZTS, on the other hand, can take two different forms. The stannite structure has the same tetragonal coordination as the stannite structure but altered symmetry due to alternate cation positioning in the crystal lattice. The structure formed from wurtzite is a hexagonal close-packed array. Although all three have the nominal Cu2ZnSnS4 stoichiometry, the kesterite structure is most commonly employed in solar cells. A promising absorber material for third-generation kesterite thin film solar cells is mixed chalcogenide CZTSSe, which has earth-plentiful components, is inexpensive, environmentally friendly, and has outstanding photovoltaic performance. A numerical simulation of p-CZTSSe/n-CdS heterojunction solar cells was provided in this work utilizing a one-dimensional Solar Capacitance Simulator. Composition, absorber thickness, defect density, and working temperature all have an effect on Voc, Jsc, FF, and power conversion efficiency.

Simulated figures and comparisons:
Energy band diagram:

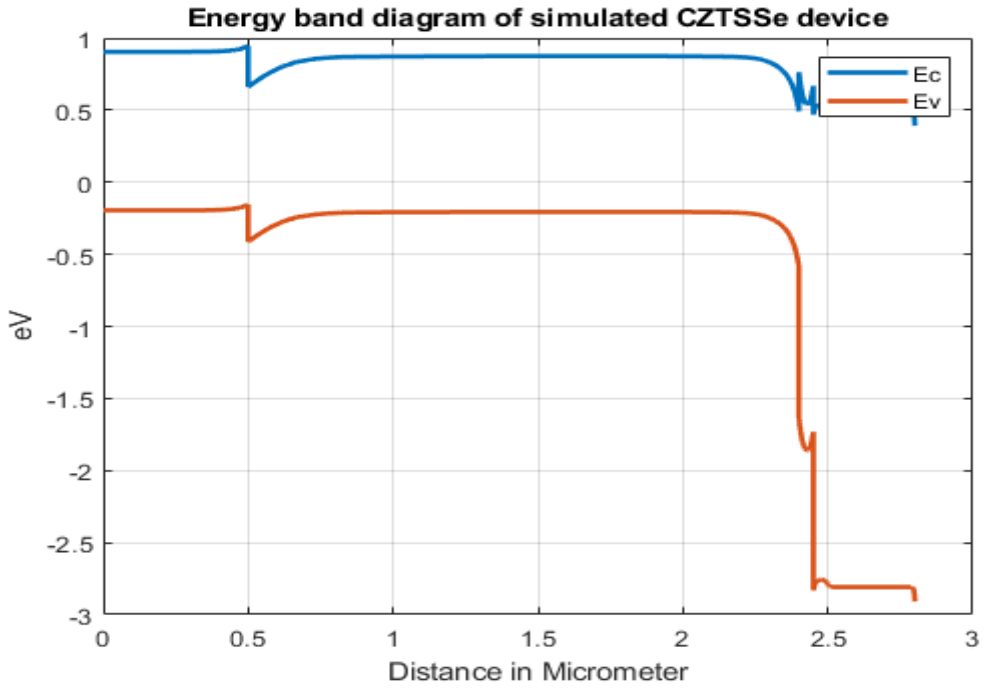

Fig. 2. Energy band diagram of simulated CZTSSe device.

One of the most fundamental physical features that determine photogenerated carrier transit, carrier recombination across the heterojunction, Fermi level splitting, and solar cell performance is band alignment. The energy difference of the conduction band can be changed by adjusting the x ratio, which can be negative or positive depending on the bandgap of the absorber layer. The whole energy band diagram under the light of our device based on the CZTSSe absorber layer generated from the SCAPS-1D simulation program is shown in Fig. 2. The conduction band minimum of the CdS buffer layer is smaller than the conduction band minimum of the CZTSSe absorber layer.

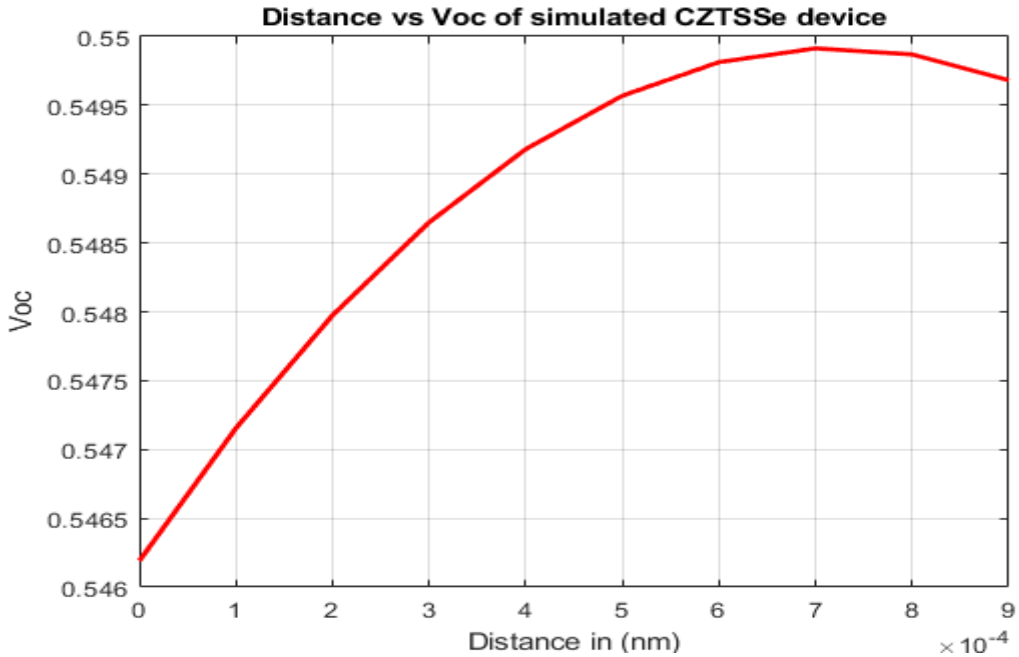

Fig. 3. Thickness vs Voc of simulated CZTSSe device.

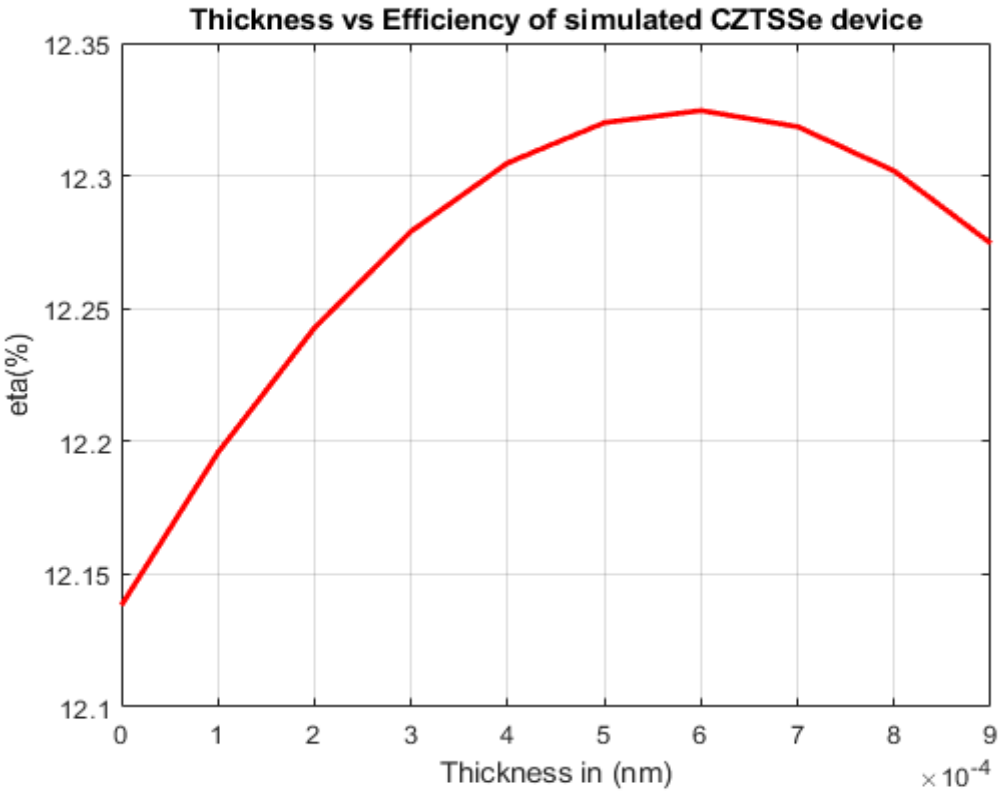

Fig. 4. Thickness vs eta of simulated CZTSSe device.

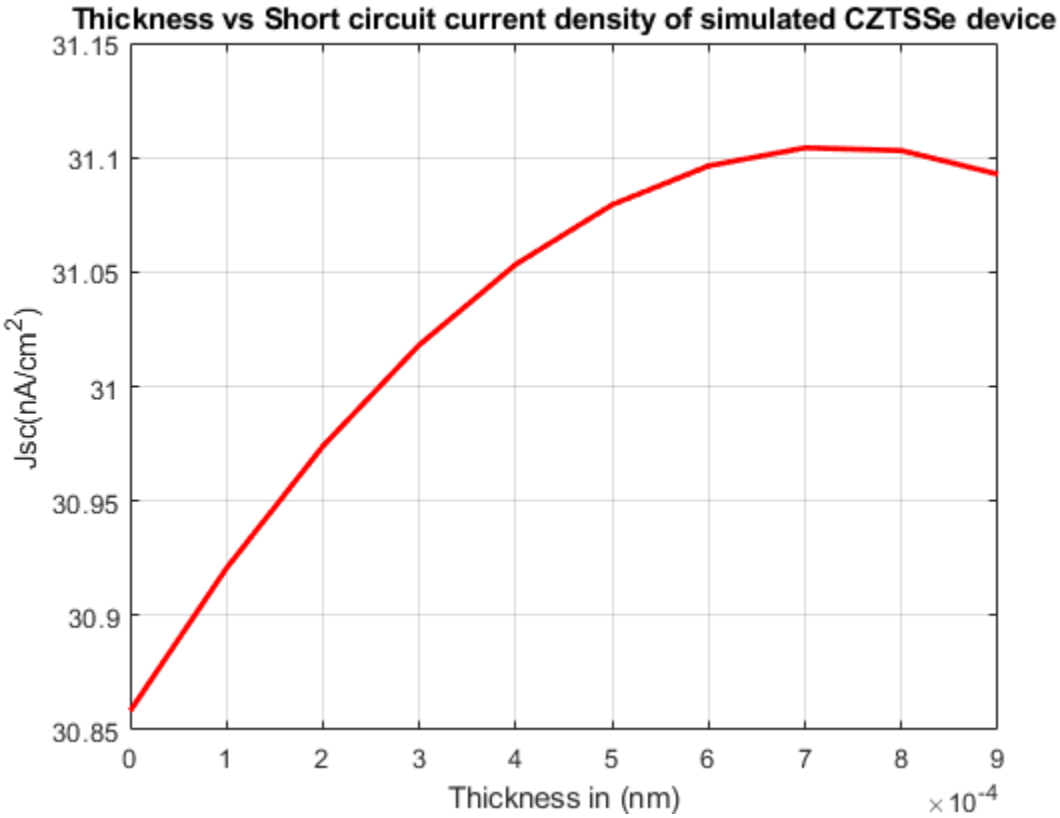

Fig. 5. Thickness vs Jsc of simulated CZTSSe device.

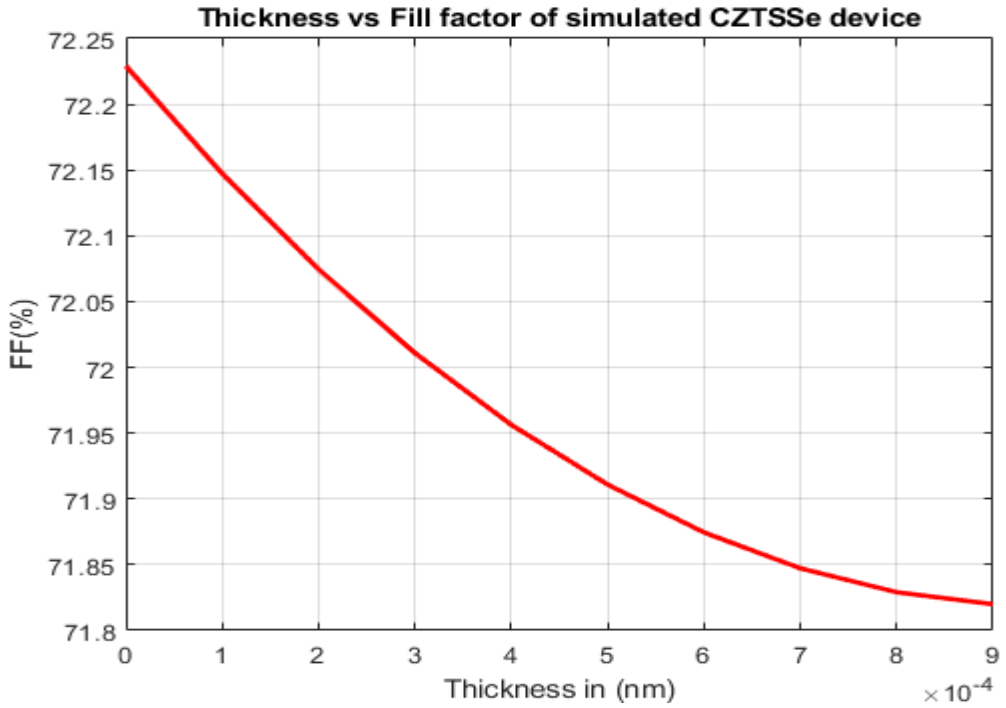

Fig. 6. Thickness vs FF of simulated CZTSSe device.

The simulation results show that as absorber thickness increases, all parameters such as Voc, Jsc, and eta rise. Only FF is decreasing. This is mostly due to the fact that as thickness increases, more photons with longer wavelengths are absorbed, resulting in the creation of more electron-hole pairs. This conclusion is consistent with Beer-Lamberts law, implying greater photon absorption in the absorber layer and the formation of additional electron-hole pairs rather than an improvement in device performance.

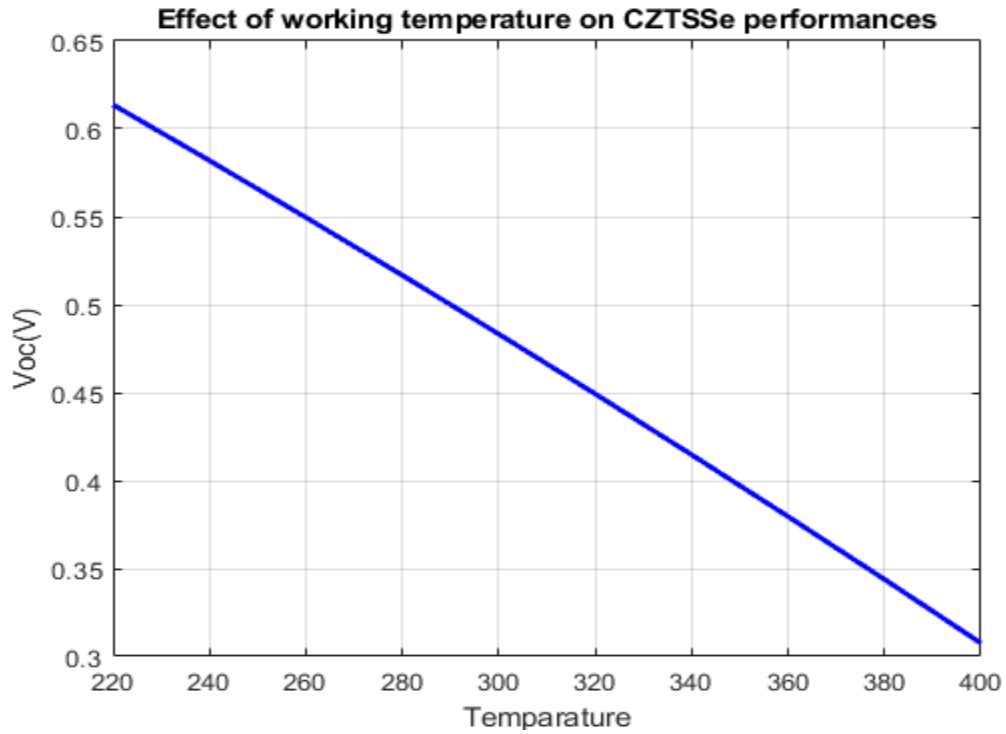

Fig. 7. Temperature vs Voc of simulated CZTSSe device.

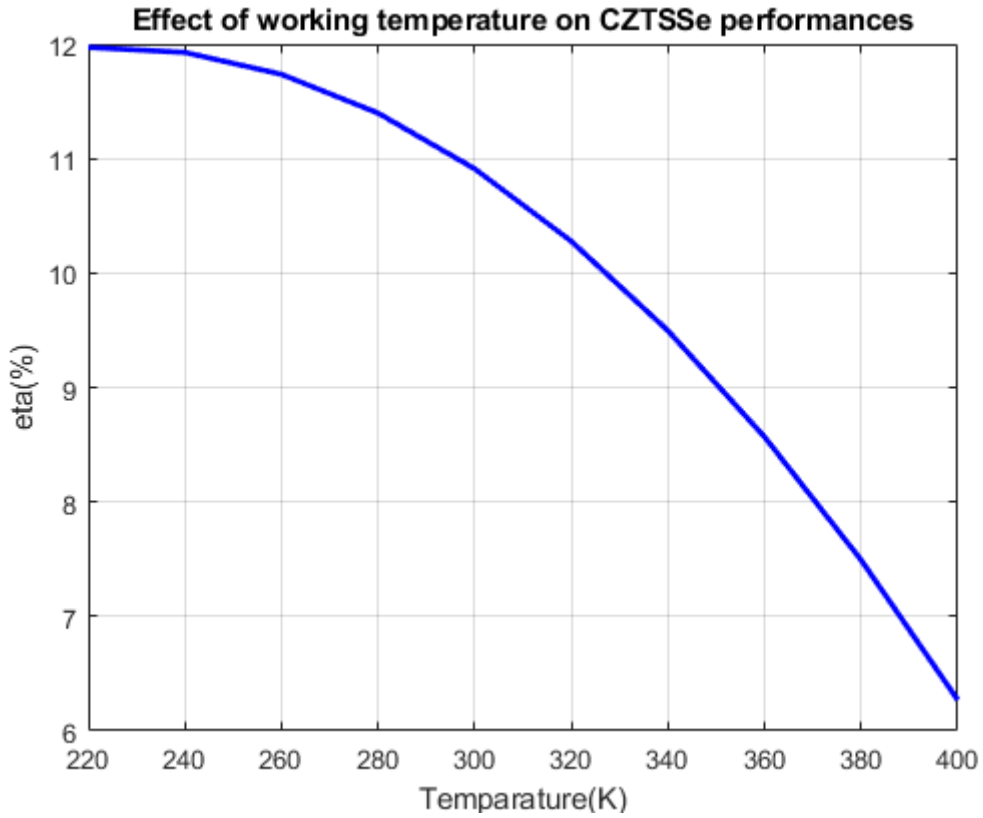

Fig. 8. Temperature vs efficiency of simulated CZTSSe device.

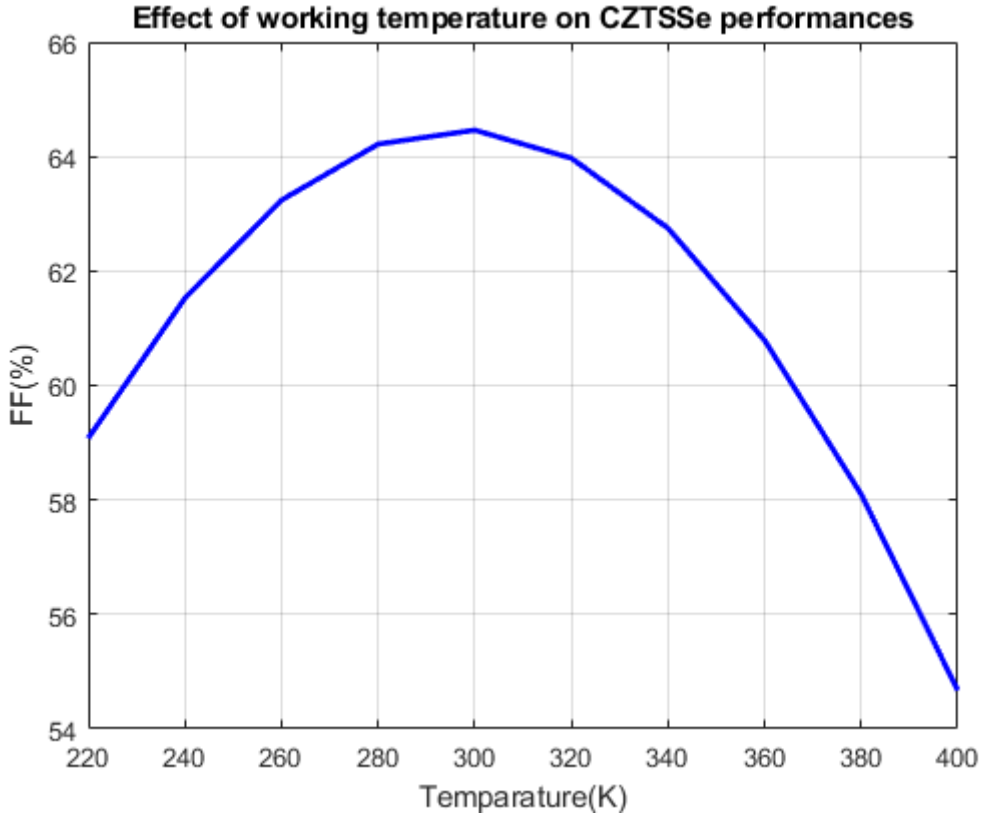

Fig. 9. Temperature vs FF of simulated CZTSSe device.

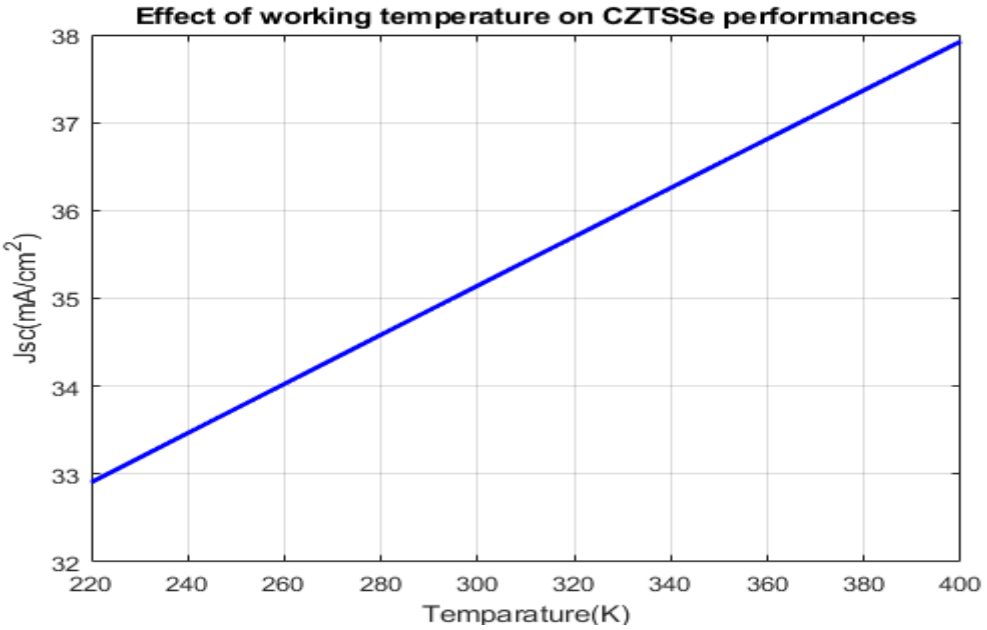

Fig. 10. Temperature vs short circuit current of simulated CZTSSe device.

Previously, all modeling investigations assumed an ambient temperature of 300 K (25 °C). But PV cell panels frequently operate at temperatures above 300 K. In this section, we looked at the effect of working temperature on the CZTSSe device performance. The simulation temperature was raised from 240 to 400 K. while maintaining other parameters constant, under a continuous illumination of 1000 W/m^2. The rise in operating temperature has been proven to influence overall device performance.

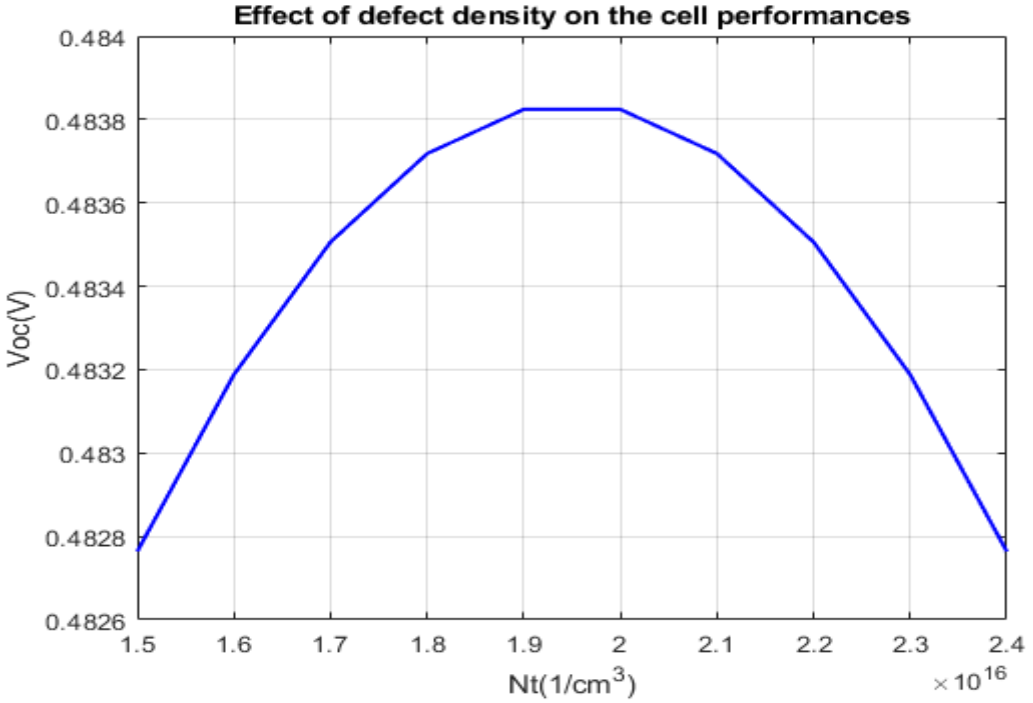

Fig. 11. Defect density vs Voc of simulated CZTSSe device.

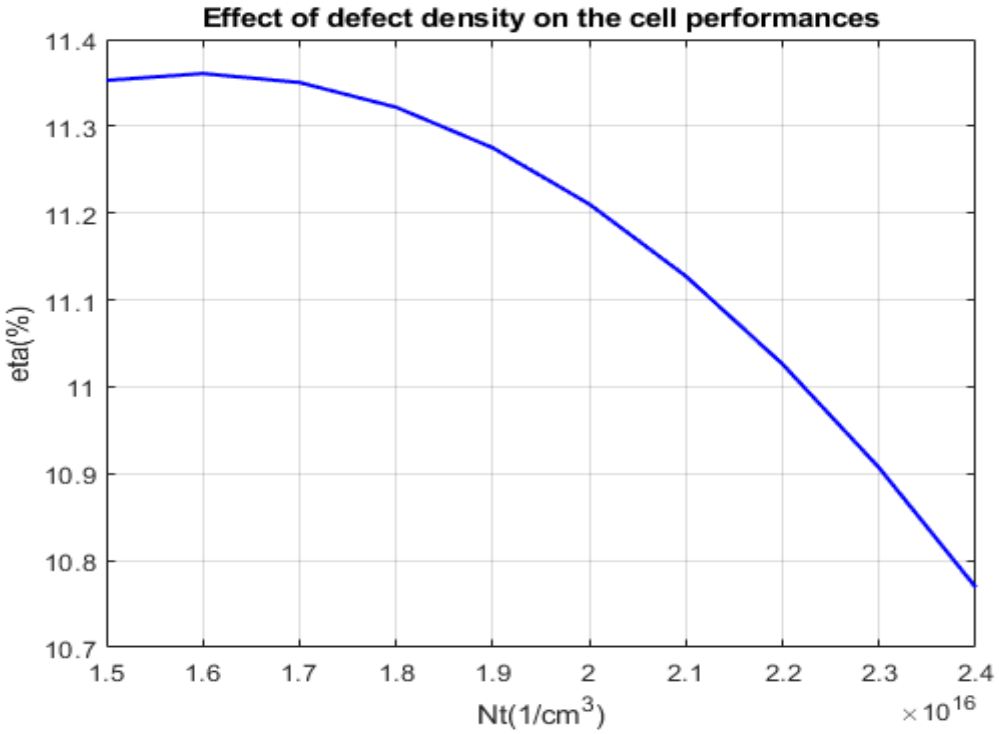

Fig. 12. Defect density vs efficiency of simulated CZTSSe device.

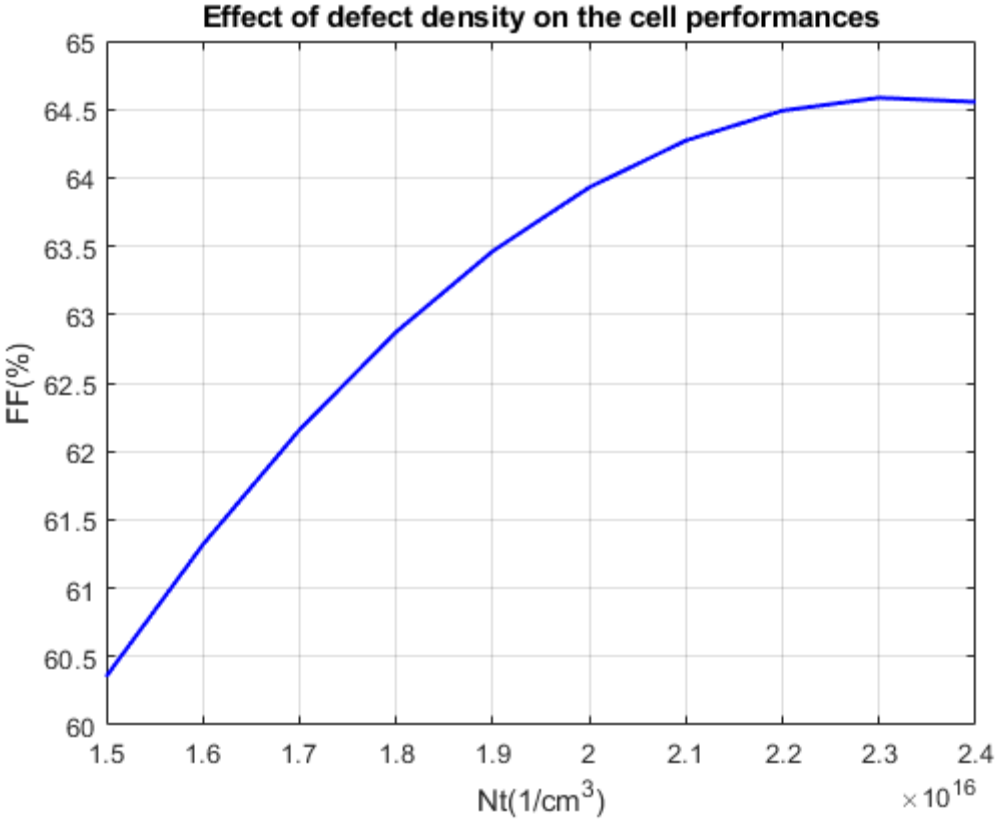

Fig. 13. Defect density vs FF of simulated CZTSSe device.

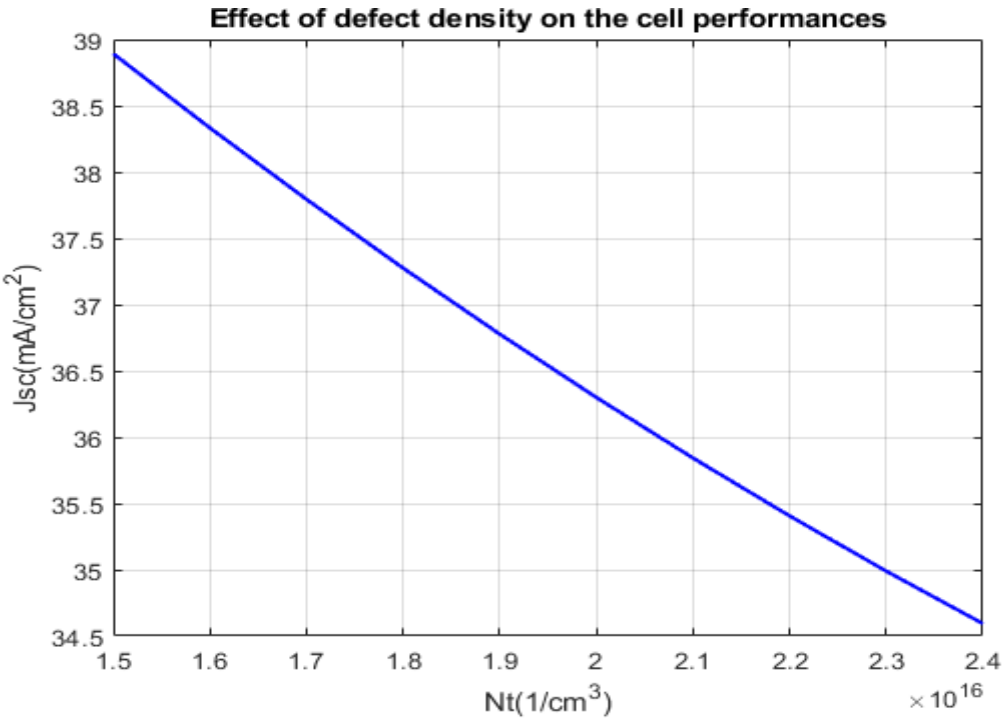

Fig. 14. Defect density vs short circuit current of simulated CZTSSe device.

The optoelectronic properties of thin film semiconductor compounds are significantly affected by defect states in bulk material and interface. These imperfections may operate as recombination hotspots for photogenerated carriers, affecting the Voc and the solar device's conversion efficiency. In Fig. 11 we can see that as the defect density increases the Voc also increases. Voc reaches its highest when defect density is 1.95 and as the Nt increases the Voc decreases. In Fig.12 and Fig.14 we can see that defect density increases efficiency and short circuit current decreases.

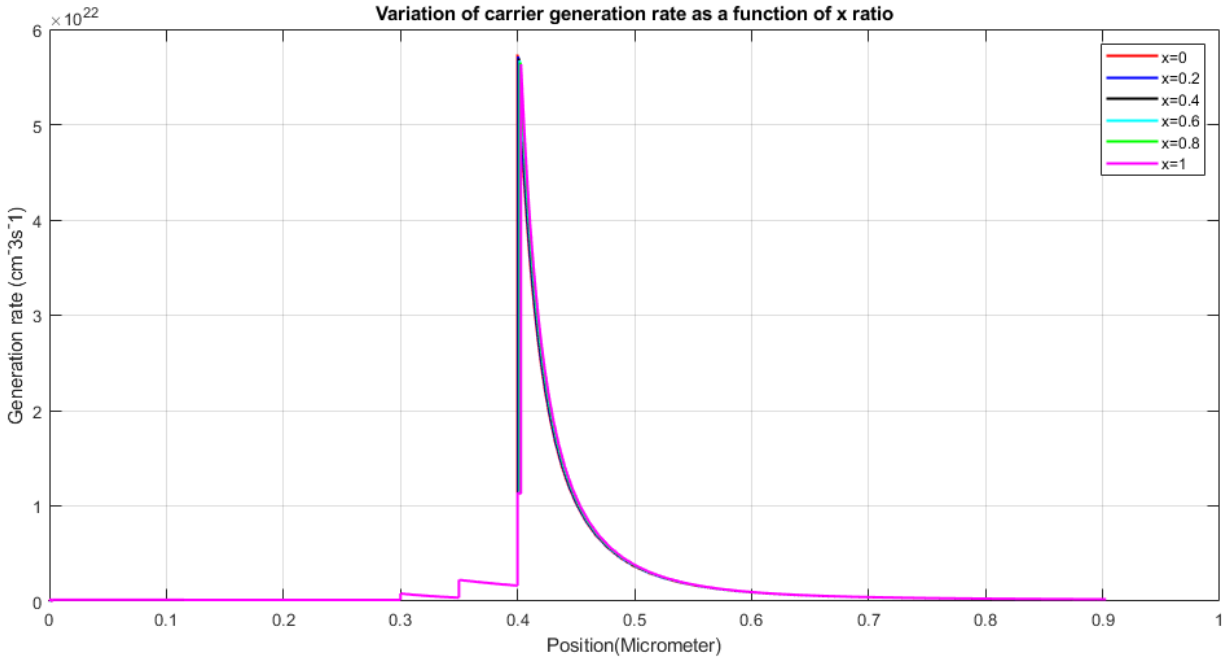

Fig. 15. Variation of carrier generation rate as a function of x ratio.

The carrier generation rate of ZnO:Al/ i-ZnO/n-CdS/p-CZTSSe/Mo cell configuration shown in Fig. 15. It can be seen that the generation rate decreases with increasing depth in the CZTSSe bulk.

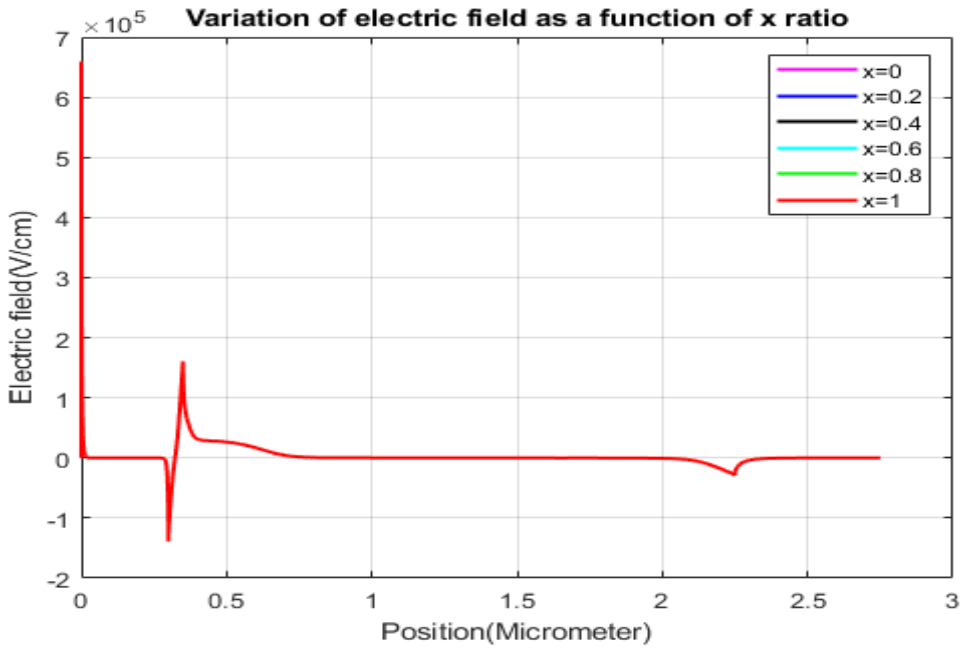

Fig. 16. Variation of electric field as a function of x ratio.

Fig.16. shows the built-in electric field of ZnO:Al/ i-ZnO/n-CdS/p-CZTSSe/Mo cell configuration. There is a strong value of the electric field at the CdS/CZTSSe interface, which drops rapidly as we go inside the CZTSSe layer.

Comparison:

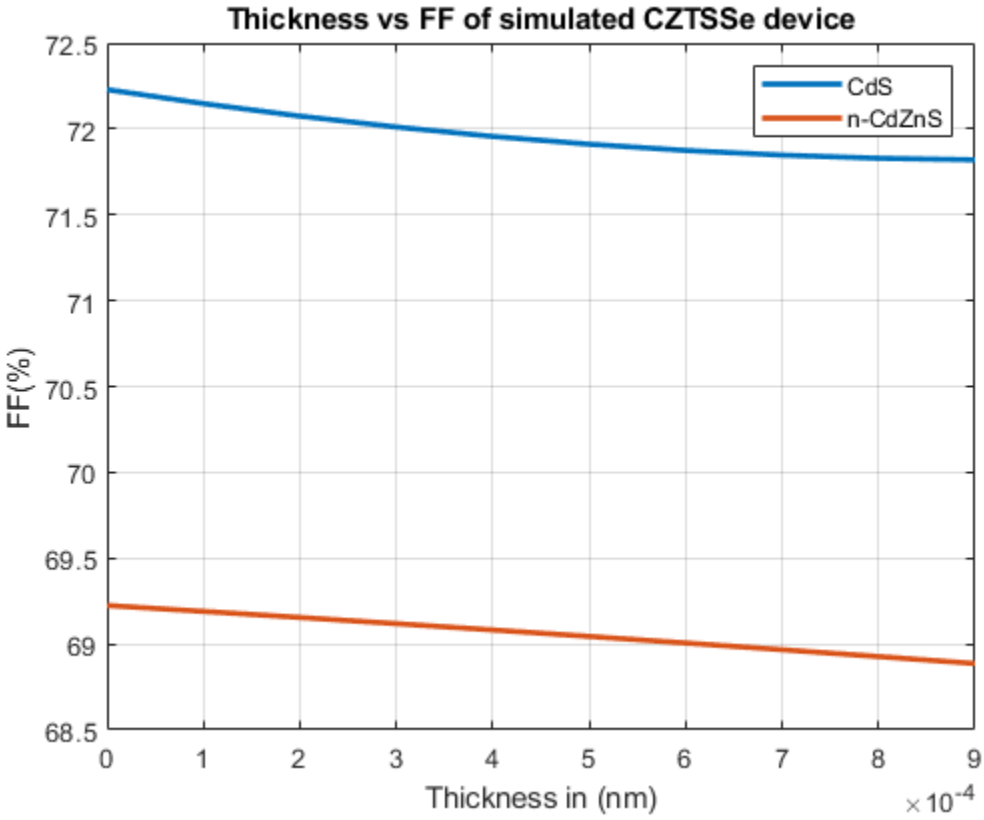

Fig. 17. Thickness vs FF of simulated CZTSSe device.

From the figure, we can see that CZTSSe shows a higher fill factor when CdS is used as buffer layer compared to n-CdZnS.

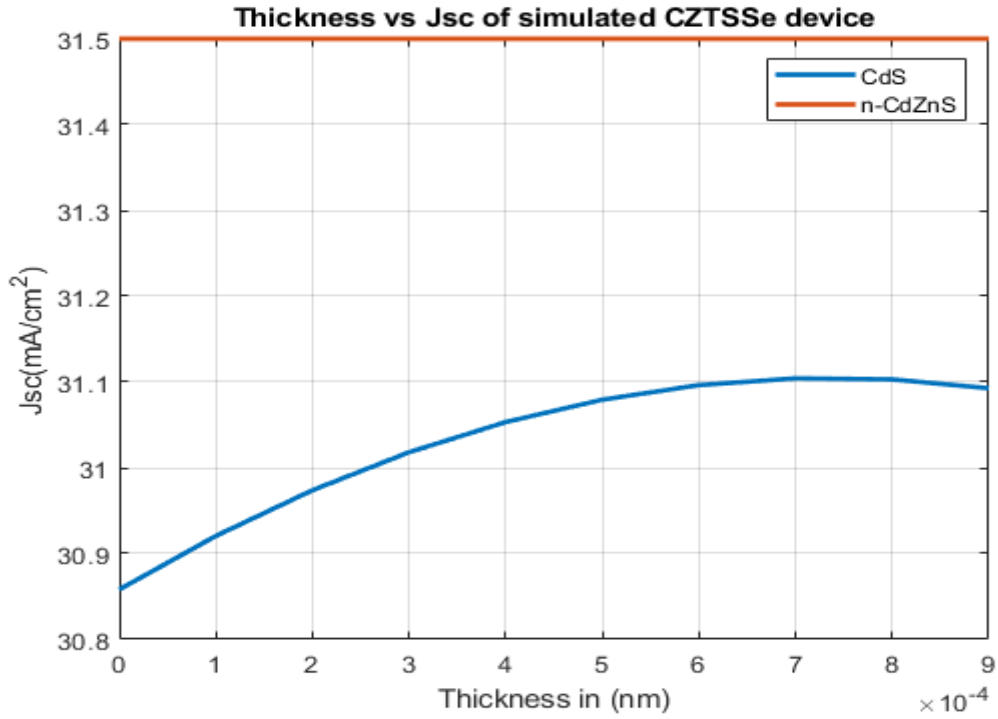

Fig. 18. Thickness vs Jsc simulated CZTSSe device.

From the figure, we can see that CZTSSe shows a higher short circuit current when CdS is used as buffer layer compared to n-CdZnS.

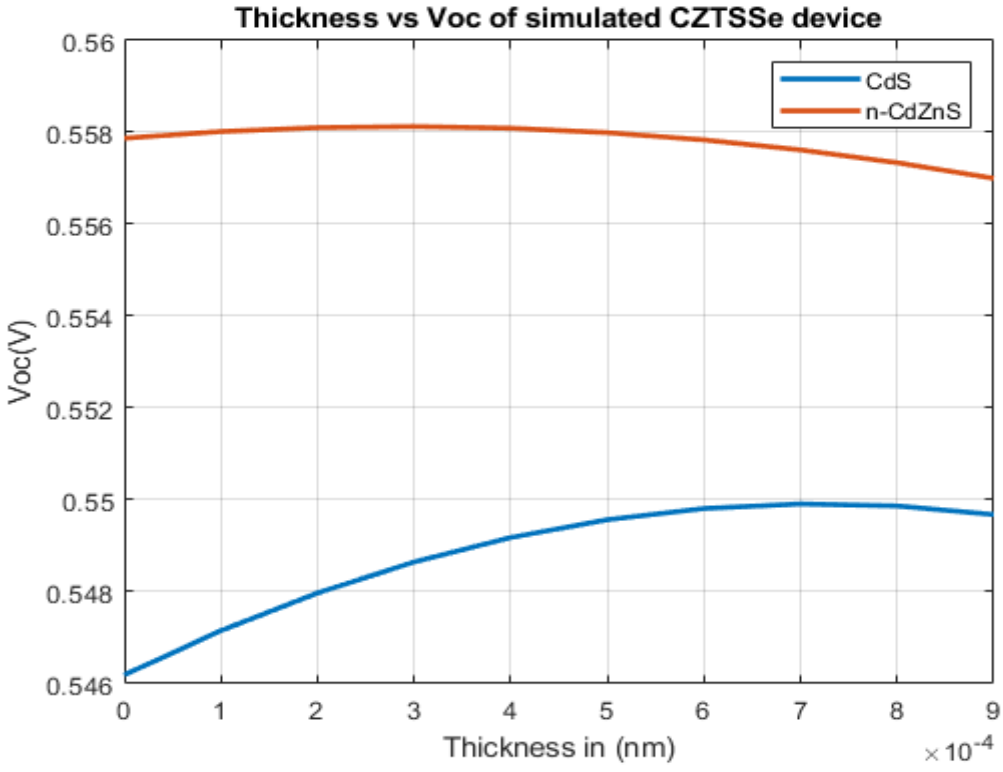

Fig. 19. Thickness vs Voc of simulated CZTSSe device.

From the figure, we can see that CZTSSe shows a lower Voc when CdS is used as buffer layer compared to n-CdZnS.

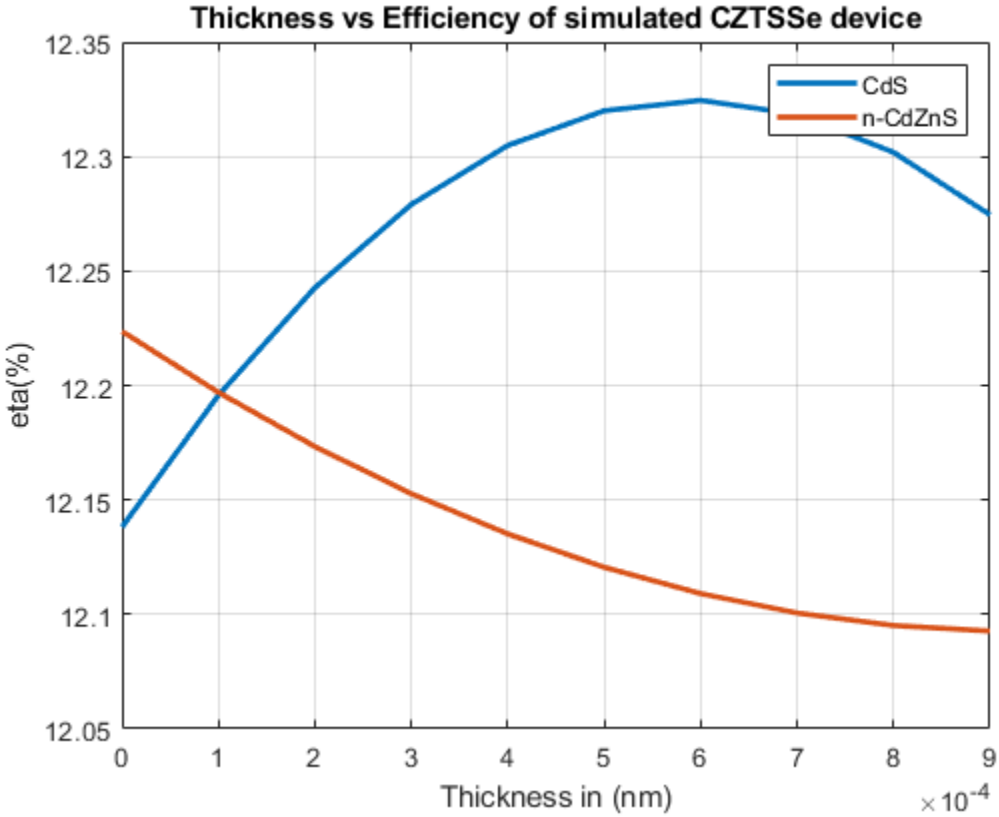

Fig. 20. Thickness vs efficiency of simulated CZTSSe device.

From the figure. 20, we can see that CZTSSe shows a higher efficiency when CdS is used as buffer layer compared to n-CdZnS.

Table 2: Comparison table of Device output variation due to increases of absorbers layer thickness of CZTSSe using $MoSe_2$ and n-CdZnS.

Material	Voc(V)	Jsc(mA/cm^2)	FF(%)	Eta(%)
CdS	0.55	31.1	72.2	12.33
n-CdZnS	0.558	31.5	69.2	12.22

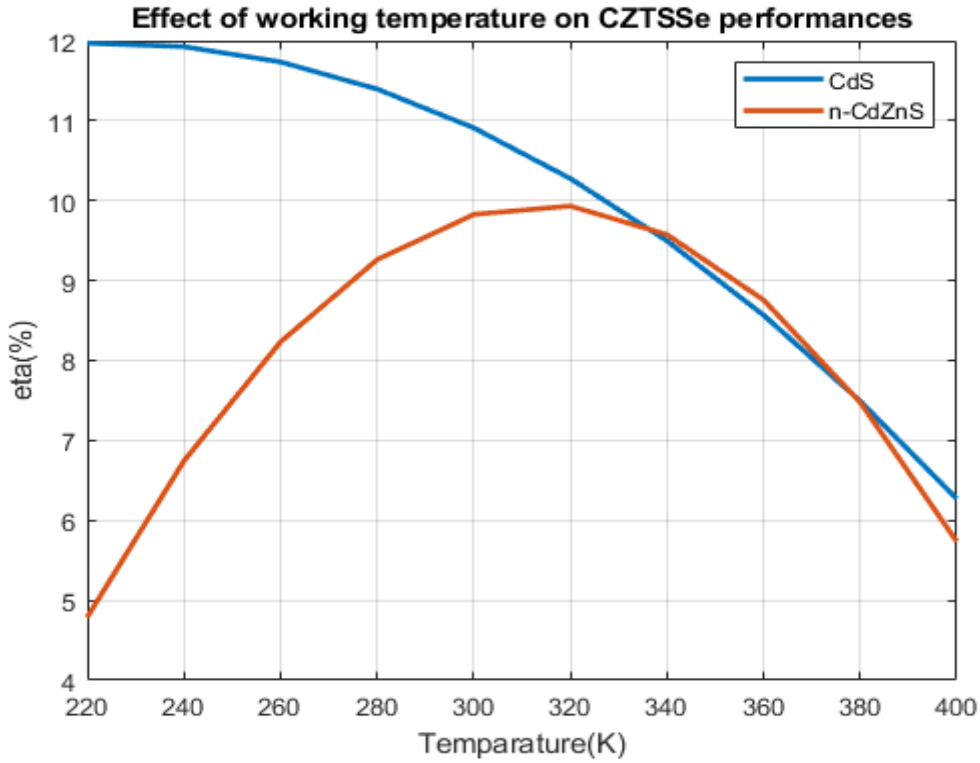

Fig. 21. Temperature vs efficiency of simulated CZTSSe device.

From the figure, we can see that we can see that CZTSSe shows a higher fill factor when CdS is used as buffer layer compared to n-CdZnS

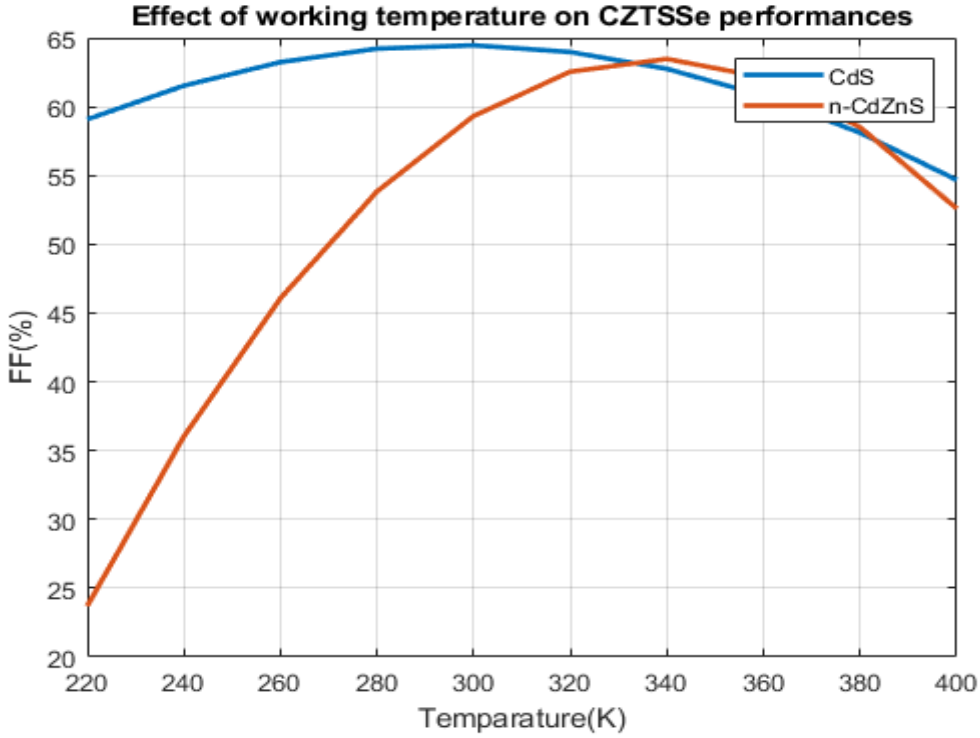

Fig. 22. Temperature vs Fill Factor of simulated CZTSSe device.

From the figure, we can see that CZTSSe shows a higher fill factor with varying temperature when CdS is used as buffer layer compared to n-CdZnS.

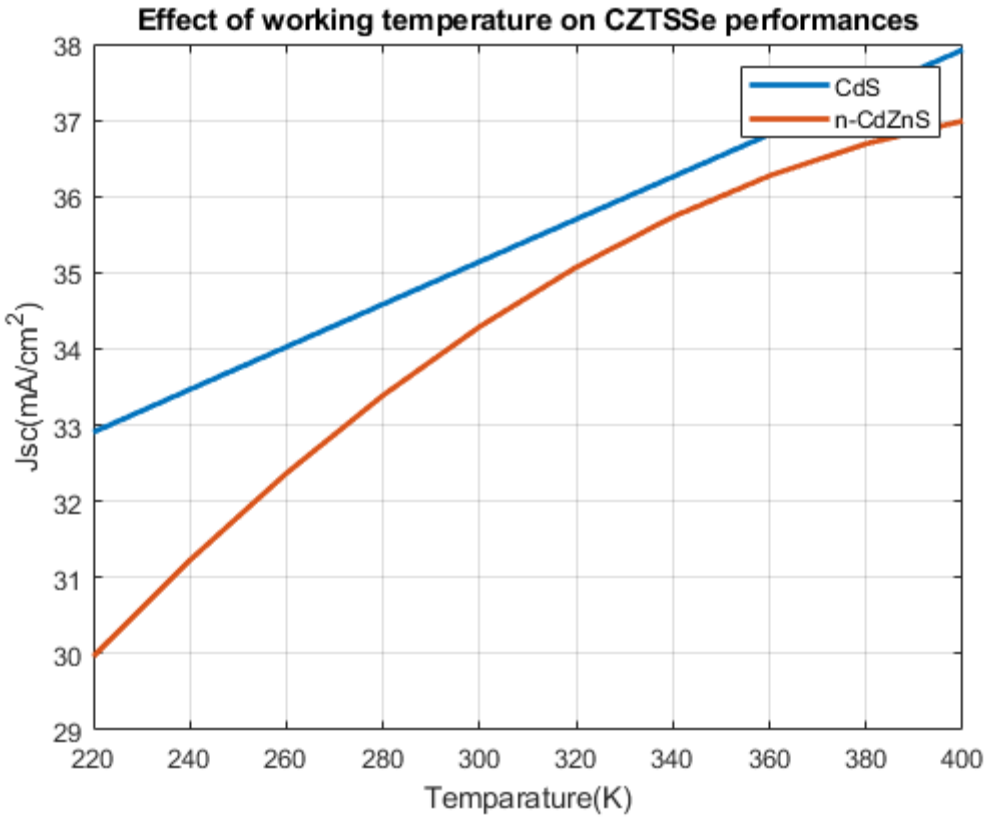

Fig. 23. Temperature vs Jsc of simulated CZTSSe device.

From the figure, we can see that CZTSSe shows a short circuit current with varying temperature when CdS is used as buffer layer compared to n-CdZnS.

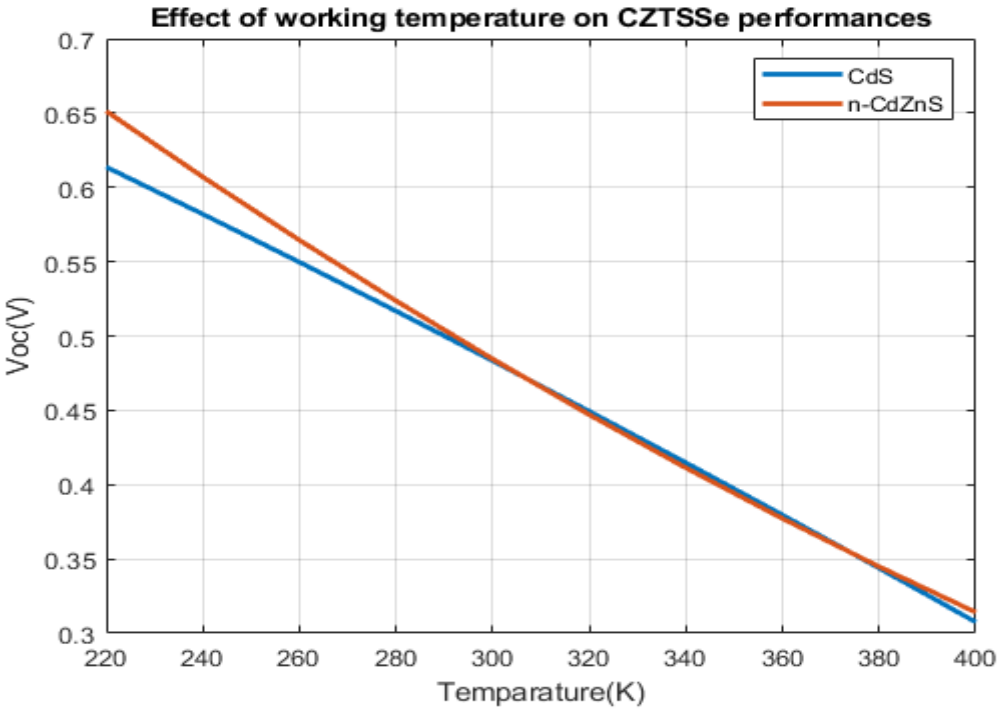

Fig. 24. Temperature vs Voc of simulated CZTSSe device.

From the figure, we can see that CZTSSe shows a lower Voc with varying temperature when CdS is used as buffer layer compared to n-CdZnS.

Table 3: Comparison table of Device output variation due to working temperture of CZTSSe using $MoSe_2$ and n-CdZnS as buffer layer.

Material	Voc(V)	Jsc(mA/cm^2)	FF(%)	Eta(%)
CdS	0.61	38	65	12.33
n-CdZnS	0.65	37	64	10.22

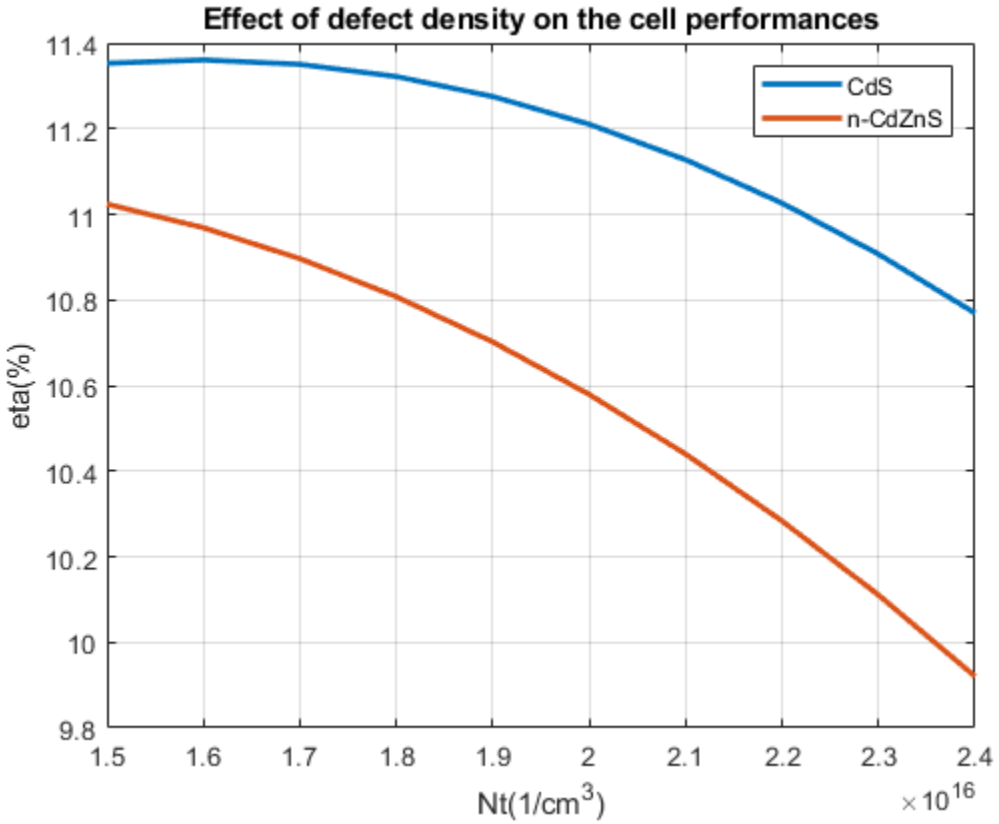

Fig. 25. Defect density vs efficiency of simulated CZTSSe device.

From the figure, we can see that CZTSSe has the highest efficiency compared to n-CdZnS when defect density is changed. As defect density increases the efficiency decreases.

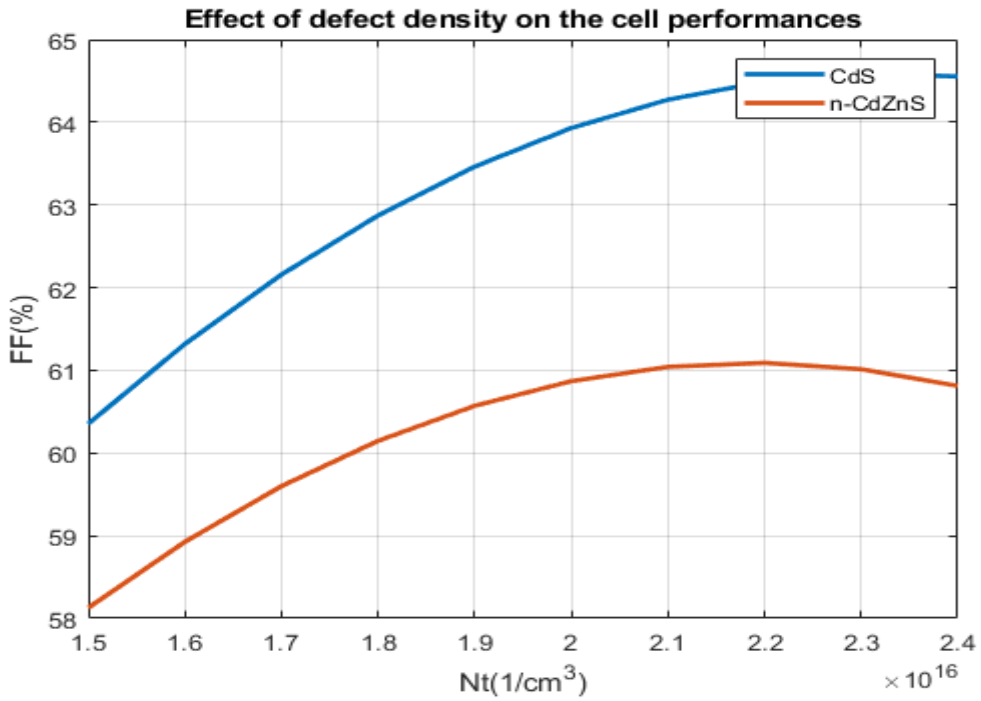

Fig. 26. Defect density vs Fill factor of simulated CZTSSe device.

From the figure, we can see that CZTSSe shows a higher fill factor with varying defect density when CdS is used as buffer layer compared to n-CdZnS.

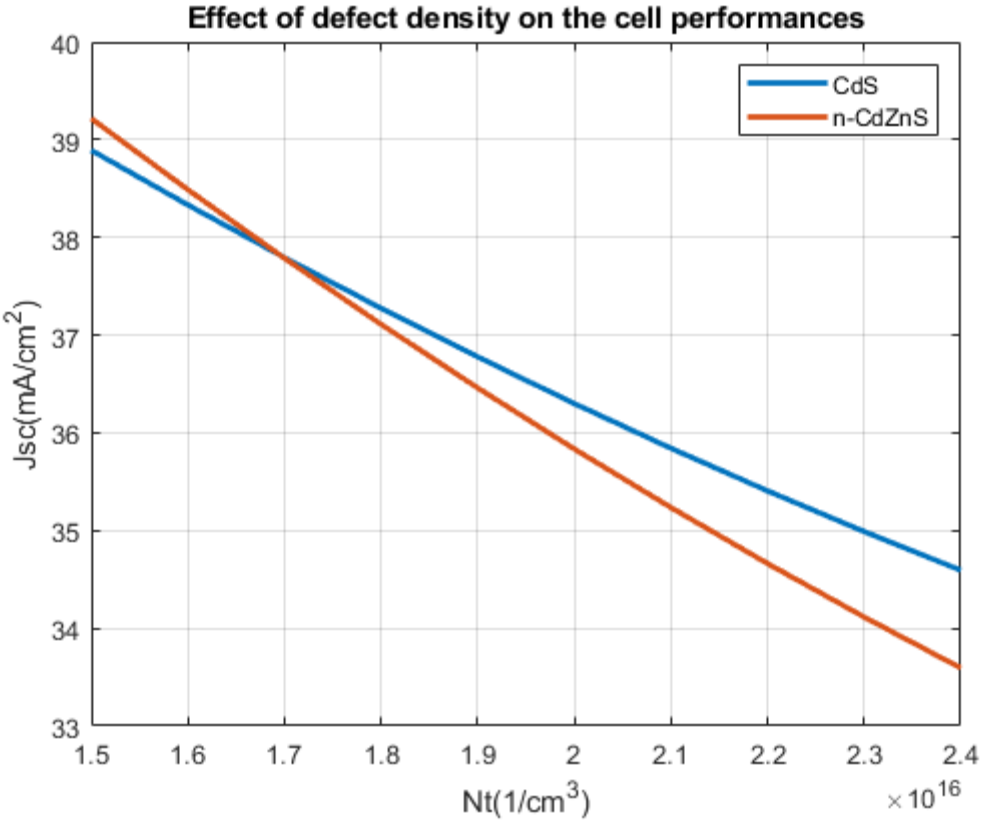

Fig. 27. Defect density vs short circuit current of simulated CZTSSe device.

From the figure, we can see that CZTSSe shows a higher fill factor with varying defect density when CdS is used as buffer layer compared to n-CdZnS.

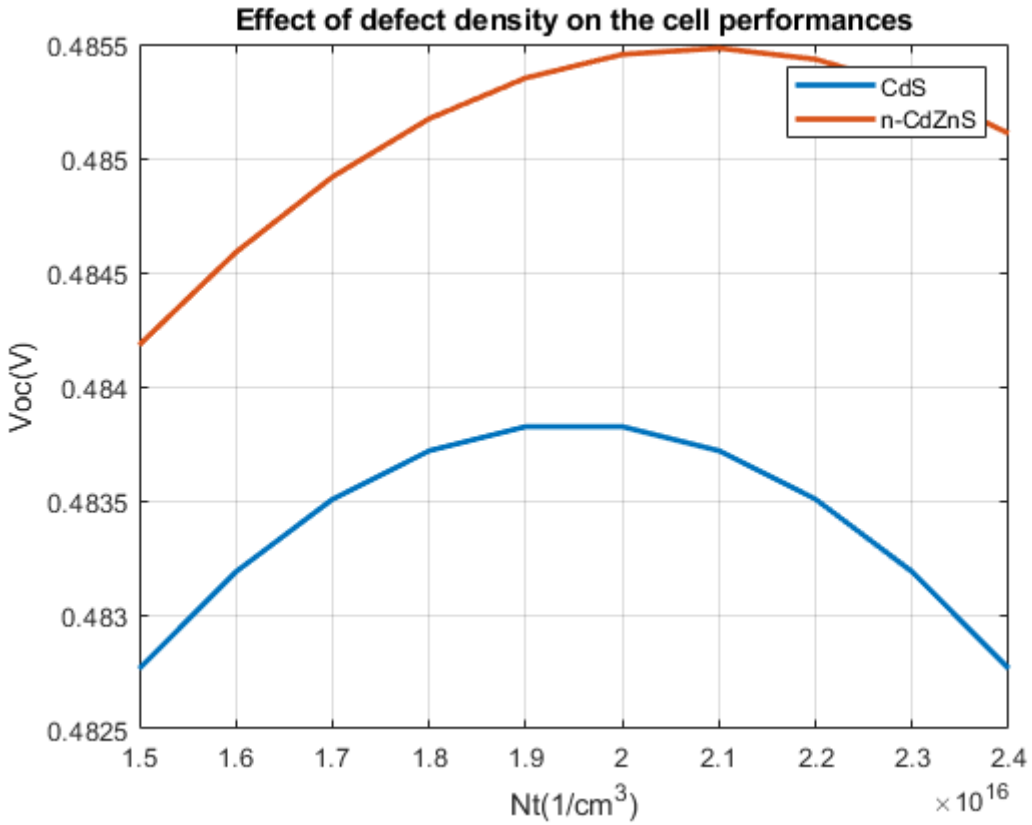

Fig. 28. Defect density vs Voc of simulated CZTSSe device.

From the figure, we can see that CZTSSe shows a slightly lower Voc with varying defect density when CdS is used as buffer layer compared to n-CdZnS.

Table 4: Comparison table of Device output variation due to defect density of CZTSSe using $MoSe_2$ and n-CdZnS as buffer layer.

Material	Voc(V)	Jsc(mA/cm^2)	FF(%)	Eta(%)
CdS	0.483	38.8	64.5	11.35
n-CdZnS	0.4855	39.2	61	11.01

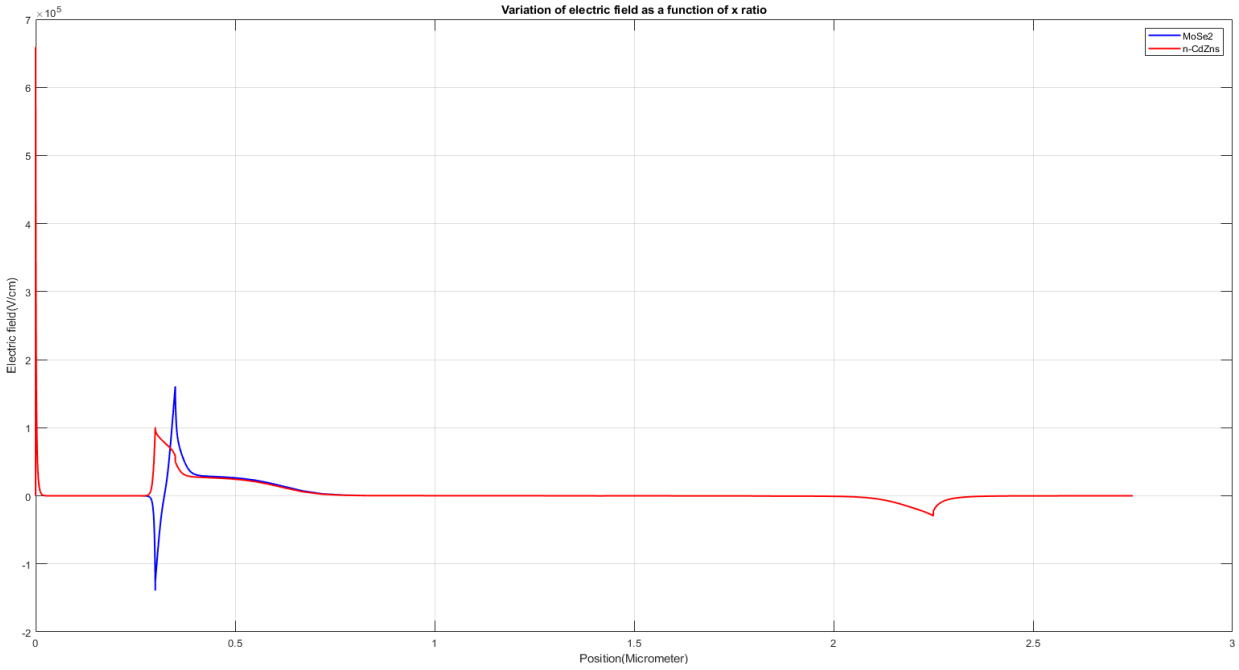

Fig. 29. Variation of electric field as a function of x ratio.

From the figure we can observe that there is a strong value of the electric field at the CdS/CZTSSe interface, which drops rapidly as we go inside the CZTSSe layer. For CdS the value goes negative when the thickness is 0.3µm and the again increases.

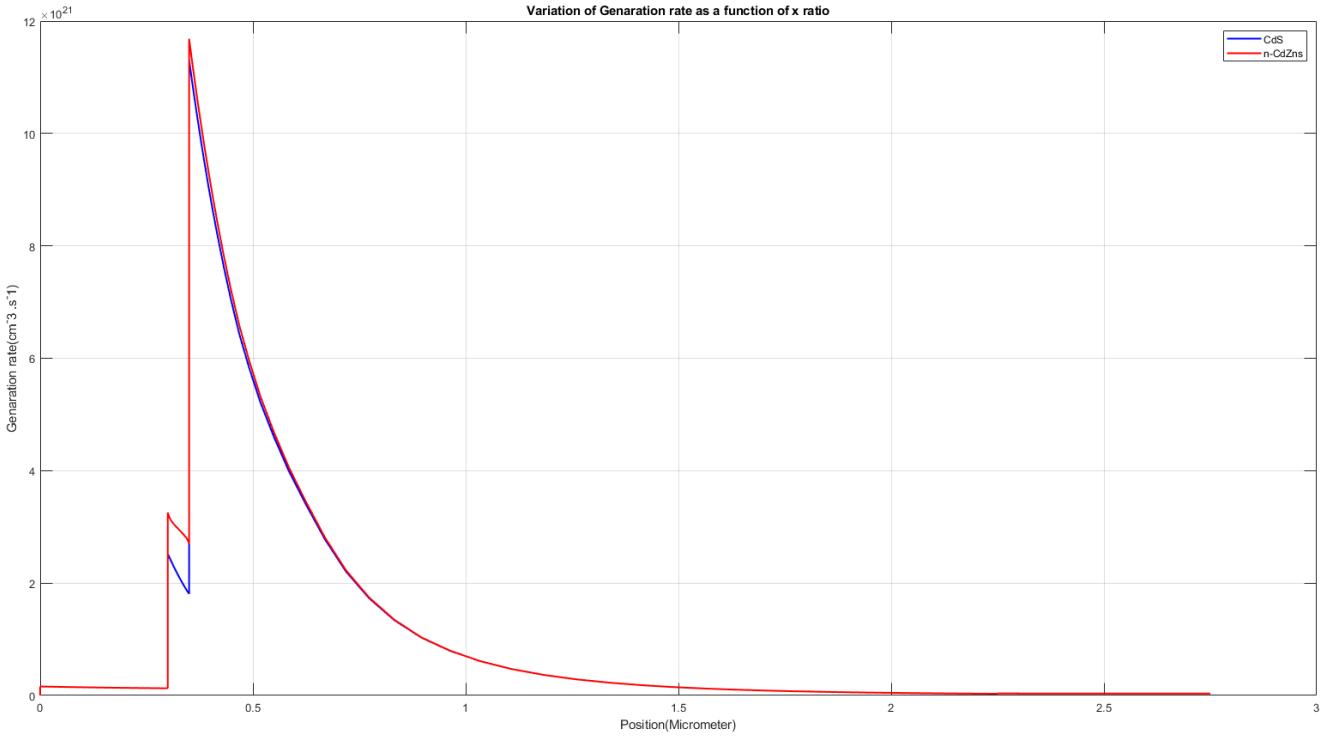

Fig. 30. Variation of carrier generation rate as a function of x ratio.

From the figure we can see that the generation rate decreases with increasing the depth in the CZTSSe bulk. The CZTSSe has a higher generation rate when n-CdZnS is used as buffer layer.

In this comparison the thickness of CdS is 50nm and the thickness of n-CdZnS is 20nm. Although the thickness of n-CdZnS is low but it shows almost similar efficiency at 280K-320K which is the optimum working condition of a solar cell. As the thickness increases the efficiency of CdZnS decreases on the other hand CdS shows higher efficiency when thickness increases. The difference of Voc is very low with compared CdS in all varied condition (Thickness, Defect density, Temperature).In varying defect density condition the Voc, Jsc FF and efficiency values have less difference.. From the comparison it can be stated that CdZnS is the better option with compare to CdS as buffer layer.

Table 5: Comaprison between experimental and simulated values.

Cell parameter	Voc (V)	Jsc (mA/cm2)	FF (%)	eta(%)
CZTSSe (Experimental)	0.521	34.98	67.2	12
CZTSSe (simulation)	0.493	35.13	64.53	10.99

Conclusion: In this assignment Numerical analysis of earth-abundant $Cu_2ZnSn(SxSe1-x)4$ solar cells based on Spectroscopic Ellipsometry results has been conducted by using SCAPS-1D software. From the simulation, we estimated the absorption coefficient for each layer using the SE values from the simulation in order to get appropriate numerical results. The performance of the third-generation solar cell is tuned for a number of controllable factors, such as composition, thickness, defect density, and working temperature, all while remaining within empirically allowed limits. In addition, the results highlight the significance of regulating the density of defects below 10-16 cm^{-3} in order to produce great output performances for TFSCs, which may be attained by regulating the production procedures. This assignment helped us to understand the selection of materials and their impact on the device's electronic properties. In buffer layer material of the CZTSSe solar cell has been changed from the approved paper and a comparison between the material of the selected paper (n-CdS) and CdZnS has been shown.